

Digital Manufacturing Process Chain for Precision Casting: A Case Study on One-Off Replacement Parts

Saidul Islam Khan¹

Hubei University of Automotive Technology, China

Mst Nishita Alam Orna²

Computer Science Engineering, Changan University, China

Md Arafat Pranto³

School of Mechatronic Engineering, China University of Mining and Technology, Xuzhou 221116, China

Md Rajauall Islam Rone⁴

School of Mechatronic Engineering, China University of Mining and Technology, Xuzhou 221116, China

A K M Redwanul Islam⁵

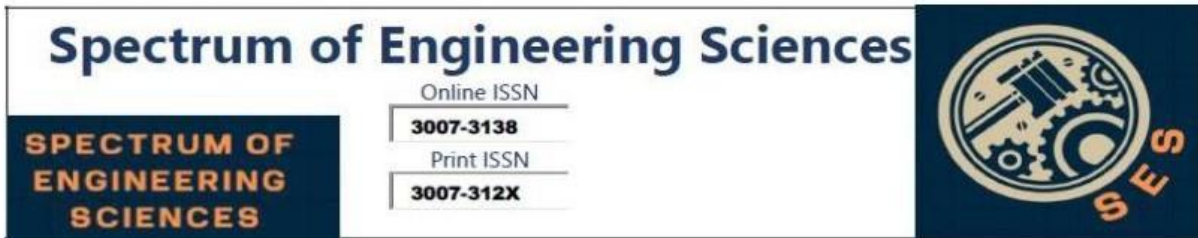
School of Mechatronic Engineering, China University of Mining and Technology, Xuzhou 221116, China

Md Mahbub Hossen⁶

School of Mechatronic Engineering, China University of Mining and Technology, Xuzhou 221116, China

Abstract

This paper investigates a comprehensive digital manufacturing process for producing one-off replacement parts using precision casting, with an emphasis on process optimization rather than technical engineering specifics. The need for such parts arises when a replacement component is unavailable due to stock shortages or discontinued production. For parts demanding intricate geometries and strict material specifications, investment casting is a suitable alternative to machining or 3D printing. The proposed process chain integrates modern technologies in a

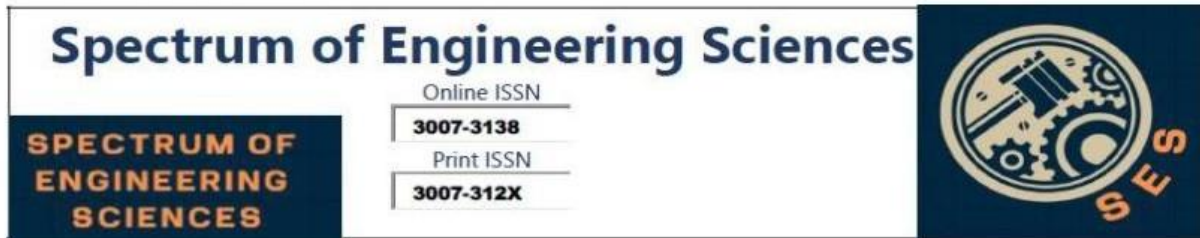


sequential and systematic manner. It begins with 3D laser scanning to accurately capture the geometry of the original part, followed by digital model creation through surface reconstruction techniques. The casting model is fabricated using additive manufacturing methods, while material properties are examined with scanning electron microscopy (SEM). Process parameter optimization is performed through casting simulations, culminating in the production of the part using a vacuum casting machine. A case study featuring a cylinder liner from a model car engine exemplifies the workflow. The methodology highlights a "right-first-time" production approach, ensuring precision and quality in a streamlined manner. Each stage of the process is critically analyzed, offering insights into key steps and identifying potential challenges. The findings underline the value of a digital manufacturing process chain in achieving efficient, high-quality results for one-off manufacturing. This study provides practical guidelines for applying this approach to precision casting.

Keywords: Precision casting, one-off manufacturing, 3D scanning, digital modeling, additive manufacturing, process optimization, casting simulation, vacuum casting.

Introduction

The replication of small mechanical components with intricate geometries and strict accuracy requirements is often more practical through casting compared to machining. Casting offers a simpler process where molten metal flows into a mold cavity, avoiding the complexities of tool paths, cutting tools, and machining operations. For low-volume or one-off manufacturing, casting becomes particularly advantageous once the mold is prepared [1].



Rapid Casting, a modern advancement over traditional casting, incorporates various techniques. Additive manufacturing (AM) is integral to this process, enabling the creation of patterns or molds, often combined with 3D scanning to digitize existing components. Casting simulations further optimize feeding system designs and process parameters, ensuring precision and efficiency [2].

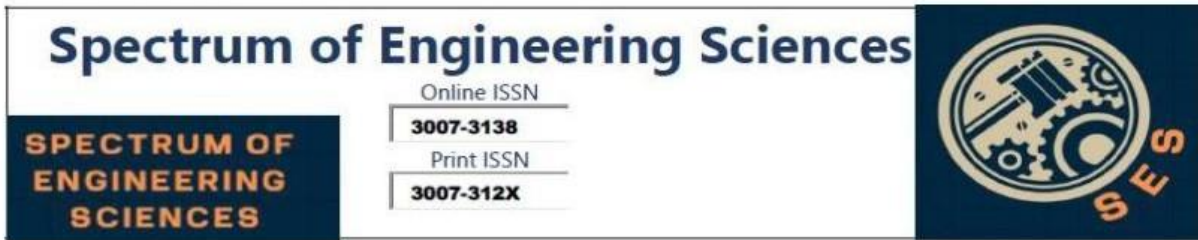
The development of AM, from its beginnings in rapid prototyping to its current capabilities in additive manufacturing, has significantly impacted the casting industry. Initially, AM was used to create patterns, which were then utilized to produce molds using materials such as Room-Temperature-Vulcanization (RTV) silicone. Over time, AM evolved to directly manufacture molds or cores, particularly for small-batch production. These processes, collectively referred to as rapid casting, offer a versatile yet efficient solution for casting applications [3].

Today, both direct and hybrid AM methods are widely used in sand and investment casting. Specialized software tools guide the selection of the most suitable manufacturing route, considering the characteristics of the target product [4].

Investment Casting is one of the most notable beneficiaries of AM advancements. Wax patterns produced using AM are invested in ceramic slurry or plaster to create molds. Despite these developments, certain challenges persist:

Layer Thickness and Positioning Accuracy: AM machines may struggle to achieve the required layer thickness or positioning accuracy, leading to shape approximations [5].

Material Limitations: Early AM patterns utilized wax or resin materials, which were not always optimal for casting. Recent



advancements in AM materials have addressed some of these issues, improving casting quality [6].

Dimensional Accuracy: The shrinkage characteristics of AM materials are often unknown, complicating predictions of final dimensions [7].

AM workflows typically require digital representations of components, commonly in STL format, generated using CAD software. Alternatively, 3D scanning technologies allow physical parts to be digitized into point clouds, which are then processed into surface and solid models. This capability supports reverse engineering, enabling the replication of parts without original blueprints. However, challenges remain in this area:

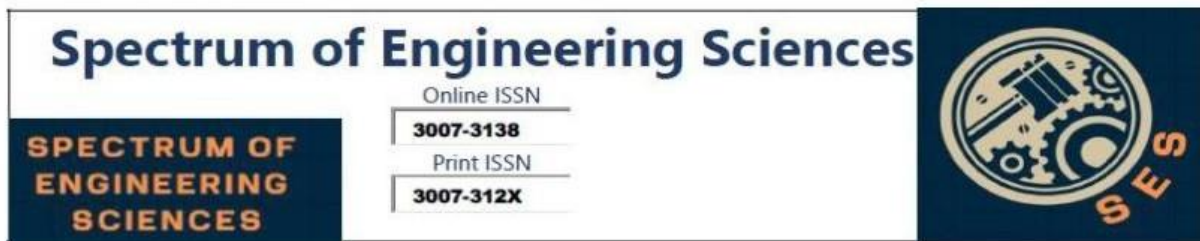
Scanning Accuracy and Coverage: Early contact scanners and laser scanners were slow and required meticulous planning. Newer optical methods are faster but less precise and struggle with occlusions [8].

Surface Fitting and Tolerance: CAD software often encounters difficulties in accurately fitting surfaces to scanned points, which can lead to dimensional discrepancies [9].

Material Analysis: Determining the material properties and microstructure of a component requires separate expertise and techniques [10].

Shrinkage Allowance: Universal shrinkage allowances are applied despite their limitations, often causing discrepancies between scanned models and final castings [11].

Casting Simulations have emerged as a powerful tool for optimizing the casting process. Simulations allow virtual experimentation with feeding systems and process parameters,



particularly for small-batch production where physical trials may be time-prohibitive. However, challenges persist:

Mesh Construction: Developing finite element meshes for simulations is labor-intensive and requires manual corrections [12].

Expertise Requirements: Simulations demand skilled operators or advanced optimization software, which is still under development [13].

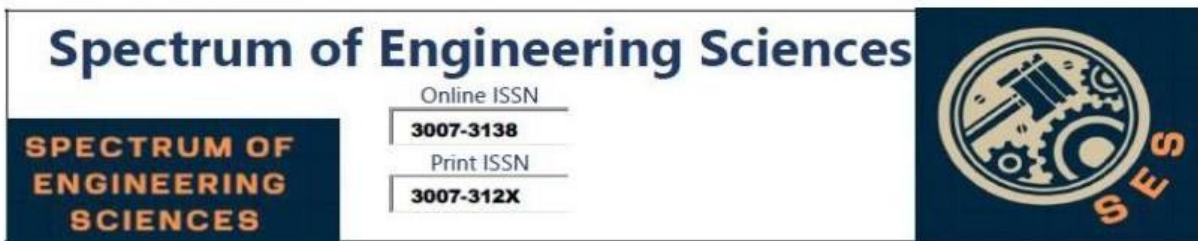
Heat Transfer Coefficients (HTCs): Accurate HTCs for specific casting materials and geometries are often unknown and must be determined through advanced software tools [14].

AM, 3D scanning, and casting simulations have found success in applications such as custom prostheses, replacement parts, and prototypes. These technologies significantly reduce the lead time for developing castings, often compressing weeks of work into days [15].

This study investigates the integration of these technologies into a streamlined process chain for rapid casting. Using a cylinder liner from a model car engine as an example, the research documents practical steps and techniques for creating high-precision one-off castings. The methodology includes:

- (1) Scanning the part using a high-precision laser scanner.
- (2) Constructing a digital model from the scanned data.
- (3) Investigating the material properties of the original part.
- (4) Simulating the casting process to optimize tools and parameters.
- (5) Implementing the casting process based on simulation results.

By addressing the challenges associated with rapid casting, this work provides a comprehensive framework for producing precise and reliable one-off castings. The replication journey



begins with scanning, which captures a point cloud representing the geometry of the original part. This is followed by surface/solid modeling to generate a digital representation of the part. Material analysis (SEM) provides the necessary specifications for simulation and modeling. Casting simulation evaluates critical indices, such as porosity, shrinkage, and solidification time, to ensure quality. Subsequently, molds are constructed based on the simulation models, paving the way for the casting process, where the final cast parts are produced. The outcome of this comprehensive process is the replicated parts, which are ready for evaluation or use (Figure 1).

From Scanning to Final Casting: A Replication Journey

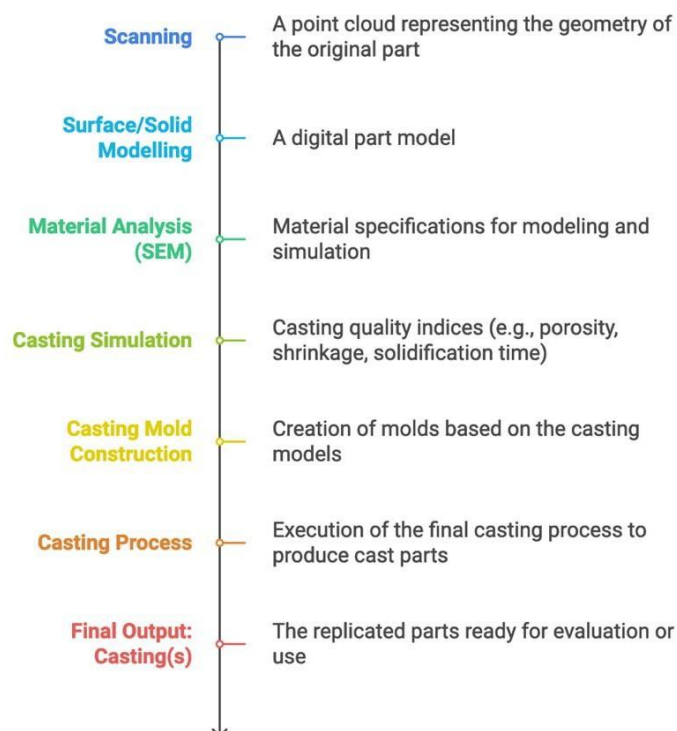
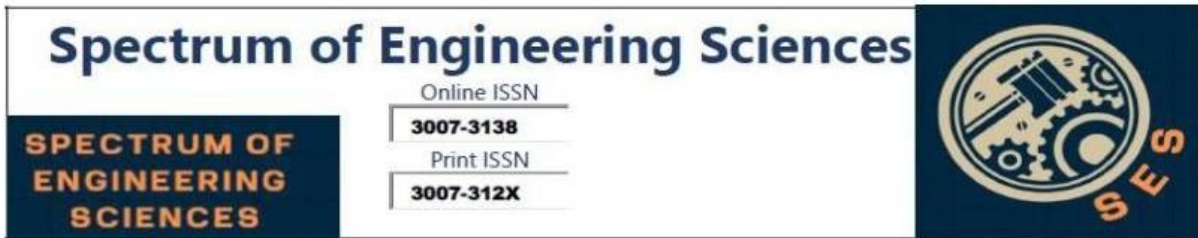


Figure 1. Processes and their outputs in one-off copy-casting.



Scanning The Part

The component selected for replication is a cylinder liner from a two-stroke model car engine. The part is a crucial element of the engine, featuring eight ports, six of which exhibit pairwise symmetry (Figure 2). These ports are integral to engine performance, directly influencing the timing and the power-speed characteristics of the engine.

In the model car racing community, it is a common practice to manually enhance the ports using a tool such as a Dremel™ (Robert Bosch Tool Corporation, Mount Prospect, IL, USA). These enhancements involve creating groove-like extensions in the ports. The purpose of these modifications is twofold:

Port Area Expansion: The extensions increase the effective area of the ports, allowing for better airflow.

Swirling Flow Enhancement: The modifications promote a swirling motion of the fuel-air mixture entering the combustion chamber. This swirling effect achieves a more even fuel distribution and facilitates the efficient expulsion of exhaust gases, minimizing fuel loss through the exhaust ports.

The specific cylinder liner selected for replication demonstrated significantly superior performance compared to its factory-manufactured counterpart. Its enhanced functionality, attributed to the modified port design, made it an ideal candidate for replication to achieve similar performance characteristics in other engines.

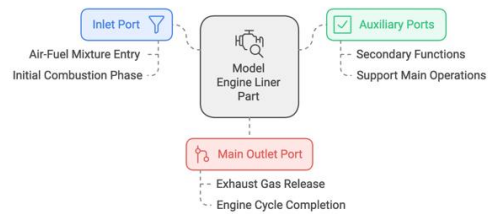


Figure 2. Model engine liner part: inlet port (A); auxiliary ports (B) and main outlet port (C) (Vosniakos, Michael, and Vasileiou 17)

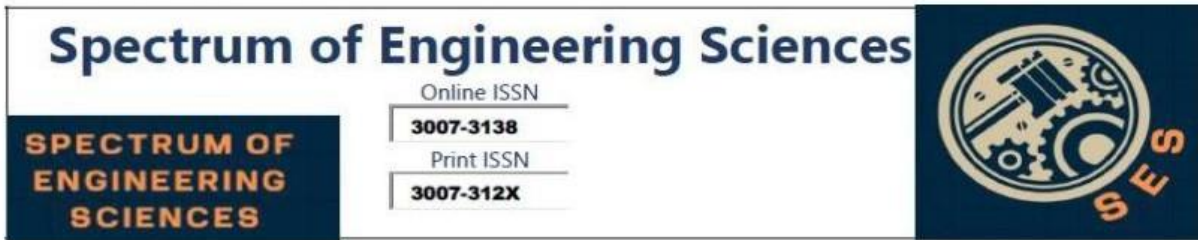
The cylinder liner selected for replication measures 30.400 mm in height, with an external diameter of 9.750 mm and an average wall thickness of 0.750 mm. The groove extensions in the ports are small, with dimensions on the scale of a few millimeters, reflecting the intricate design of the part.

Tight tolerances are critical for the liner's functionality. The radial allowance between the piston and liner typically ranges from 20 to 35 μm , while the allowance between the cylinder and liner is negative. These tolerances suggest that certain adjustments are necessary post-casting:

Outer Diameter: A light finish-turning operation may be required to ensure the correct fit.

Inner Diameter: The as-cast inner diameter is likely to be within acceptable limits, negating the need for extensive machining.

Regarding the ports' shape, a deviation of approximately 100 μm is deemed acceptable, as confirmed through consultations with model car engineers. This tolerance provides a balance between maintaining high performance and allowing for practical manufacturing feasibility. These precision requirements underscore the need for accurate scanning and subsequent replication processes to achieve the desired performance standards.



Scanning Process

The cylinder liner was scanned using a Hawk™ laser scanner with a Nextec™ laser head. For parts requiring multiple orientations, the component was mounted on a reference frame with three spheres of known diameter to maintain consistent position and orientation relative to the scanner's global coordinate system (Figure 3).

The scanning process used five path definitions Rectangle, Arc, Polyline, Wideline, and Polygon tailored to the part's geometry. The sensor dynamically adjusted its position to optimize scanning conditions: retracting to avoid collision when too close, and advancing to improve accuracy when too far, though this may reduce point cloud density and increase noise.

Resolution settings were defined in two directions:

Longitudinal (Scan Path): 0.01 mm to 0.3 mm

Lateral (Perpendicular to Scan Path): 0.03 mm to 1 mm

Resolution was adjusted based on feature complexity, with simpler features requiring lower resolution. Scanning time was influenced by the resolution, with high-resolution scans (0.03×0.03 mm) taking about 50 minutes for a $10 \text{ mm} \times 10 \text{ mm}$ area. This adaptive scanning process ensures accurate capture of the part's geometry for modeling and analysis.

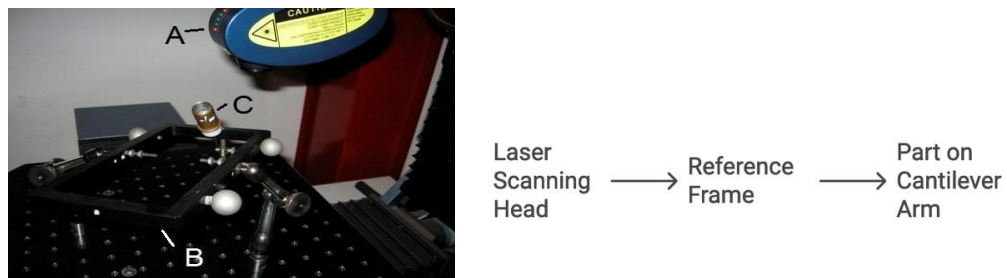


Figure 3. Laser scanning: head (A); reference frame (B) and part mounted on cantilever arm (C) Vosniakos, Michael, and Vasileiou 17)

The scanning setup for the cylinder liner (Figure 3) includes:

Laser Head (A): Captures the geometry.

Reference Frame (B): Defines the local coordinate system with spherical markers.

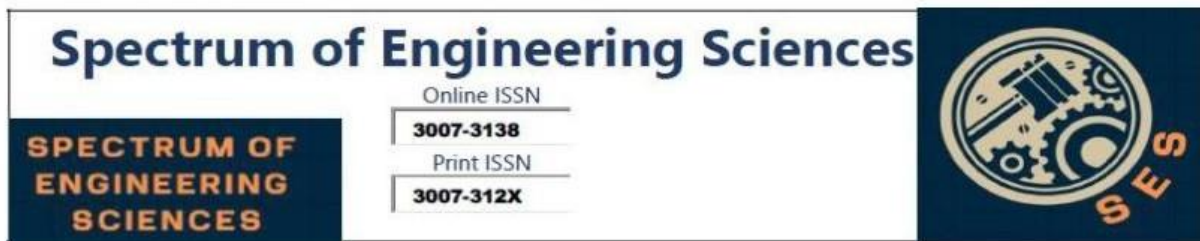
Mounted Part (C): Positioned on a cantilever arm for full access.

Setup Adjustments: A cantilever arm was added to address frame obstructions, enabling comprehensive access but increasing collision risks.

Challenges: Complex geometry required multiple orientations, reflective surfaces reduced scan quality, and selective scanning minimized time while ensuring dimensional accuracy.

Point Cloud Data

The resulting point cloud, shown in **Figure 4**, highlights the captured geometry of the liner. The data set does not encompass the entire part but focuses on critical regions required for replication and modeling. Despite the challenges, the adopted setup and scanning methodology successfully captured high-



fidelity geometric data for the most important features of the cylinder liner. This selective and adaptive approach ensured an efficient balance between scanning time and data quality, making it suitable for subsequent modeling and manufacturing stages.

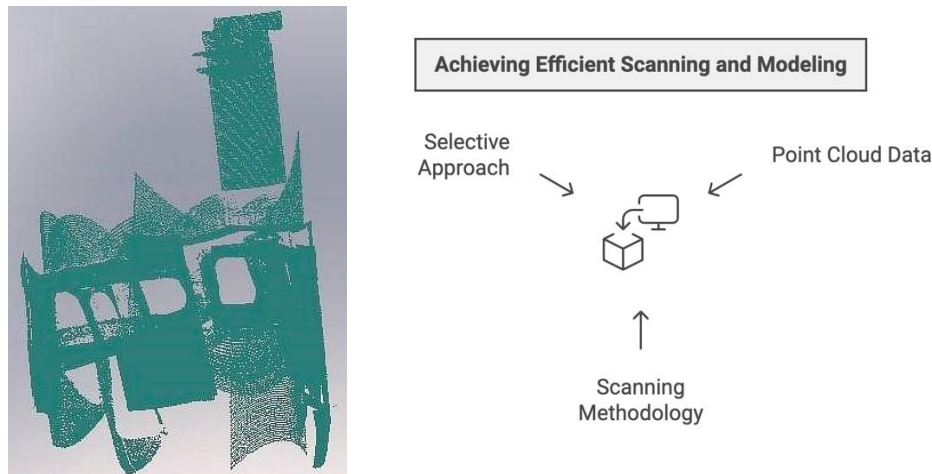


Figure 4. Point cloud (Vosniakos, Michael, and Vasileiou 17)

Digital Part Model

The point cloud generated from the scanning process was imported into SolidWorks™ using the Scan to 3D plugin to convert it into a usable surface and solid model. The model was intended for digital simulations of feeding systems and casting model fabrication.

Initial Point Cloud Processing: Due to challenges like surface reflectivity and incomplete coverage, noise reduction was performed manually to preserve critical data. Group selection tools were used to eliminate outliers while retaining important details.

Mesh Fitting: An initial mesh was generated automatically (Figure 5a), but voids in the mesh were manually repaired. The incomplete point cloud required a flexible, manual approach to ensure accurate surface extension and adjustments.

Surface Identification and Classification: The mesh was divided into surface sections, each assigned a different color for easier

visualization (Figure 5b). Surfaces were classified as **Plane**, **Cylinder**, **Cone**, or **B-spline** to facilitate accurate geometry representation.

Computational Challenges: Handling the entire point cloud was computationally demanding, slowing progress. The lack of incremental saving further hindered efficiency. Despite these issues, the final digital model accurately represented the part, enabling reliable simulations and casting model creation.

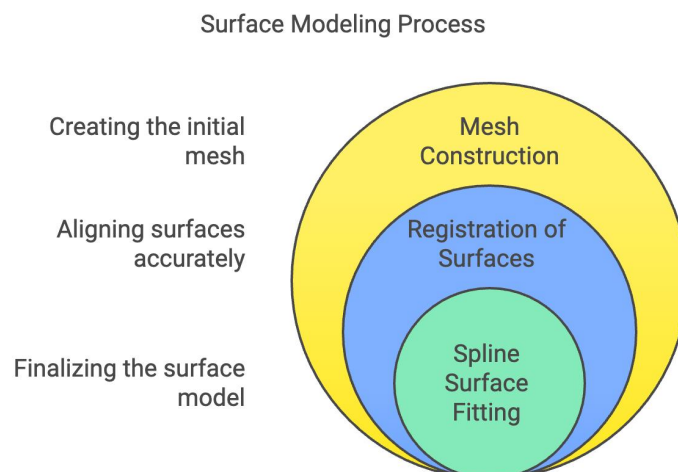
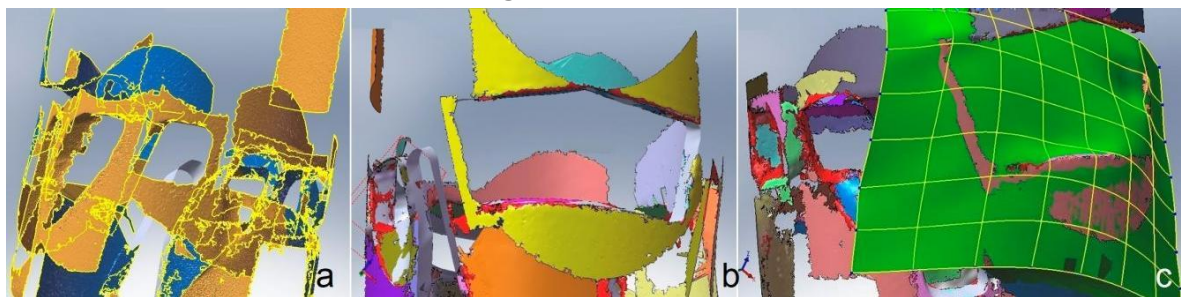
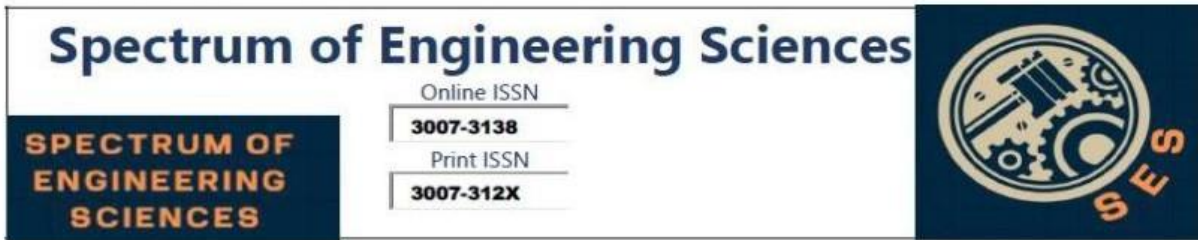


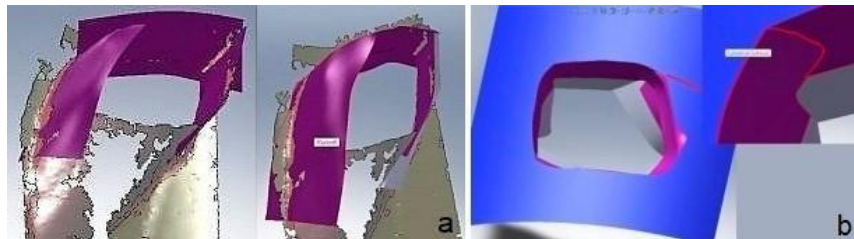
Figure 5. (a) Mesh construction (b) Registration of surfaces through painting (c) Spline surface fitting (Vosniakos, Michael, and Vasileiou 17)

Modeling the cylinder liner presented challenges, particularly with the ports. Each port side had to be defined as an individual spline surface, requiring extension, trimming, and knitting (Figure



6a). This process was labor-intensive and prone to issues, such as difficulties in extending surface patches, wrinkles during extension, and failure of surfaces to intersect, often necessitating additional patching (Figure 6b). To improve accuracy, an alternative method was employed: selecting points defining the port's outer profile to create profile splines. While this was tedious, it allowed precise control over the geometry. For complex features, intermediate profiles were added and guiding rail lines were used to prevent wrinkles when extending surfaces inward (Figure 7a, 7b). A surface lofting operation produced the final port surfaces (Figure 7c), and symmetrical ports were mirrored for consistency. For the cylinder

liner's main wall, the outer surface was modeled as a cylinder with a radius of 9.75 mm, while the inner surface was a cone with a radius ranging from 8.096 mm to 8.223 mm and a height of 25.31 mm. The space between the cylinder and cone was filled, and surfaces were knitted to form a solid. For the ends, spline curves were fitted to the point cloud data to define conical and rectangular flange surfaces, which were revolved to create the final geometry (Figure 8). The completed model (Figure 9) was saved as a binary STL file with a deviation tolerance of 0.013 mm and an angle tolerance of 5 degrees.

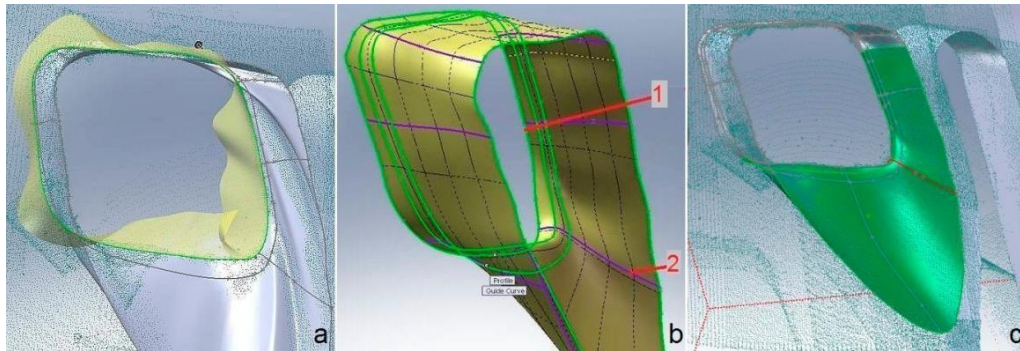


binary STL file

deviation
toleranceangle
tolerance

model

Figure 6. Port surface fitting (a) extension and trimming of separate surfaces; (b) discontinuities. (Vosniakos, Michael, and Vasileiou 17)



Port Modeling Process

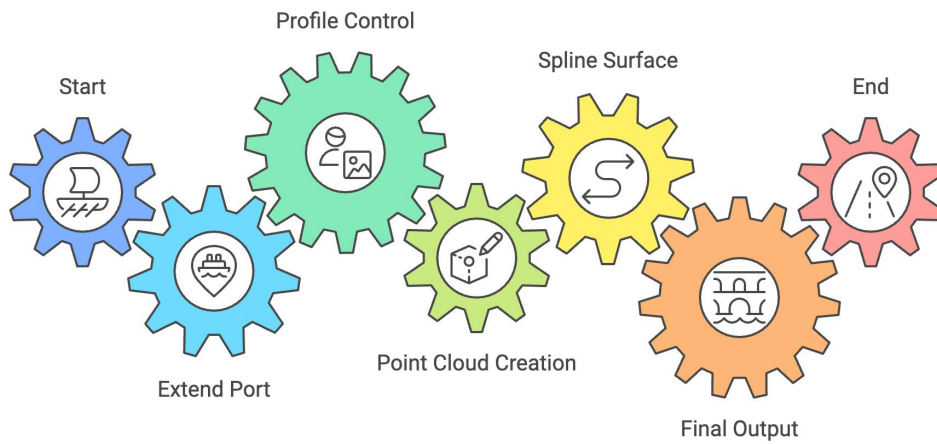


Figure 7. Port modeling (a) Extension of port entering the void volume; (b) Profile (1) controlling surface shape and guiding lines (2); (c) Part of point cloud with spline profiles, spline guides and lofted spline surface (Vosniakos, Michael, and Vasileiou 17)

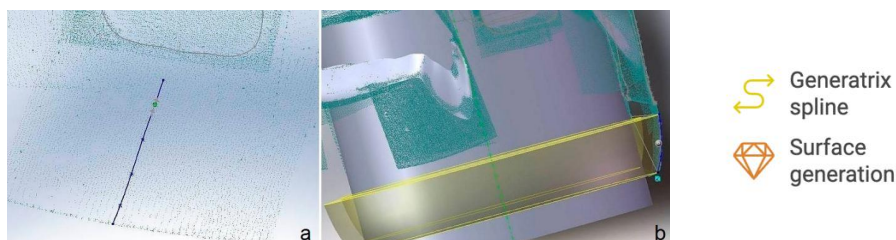


Figure 8. Modeling the lower conical area of the part **(a)**Generatrix spline construction; **(b)** Surface generation (Vosniakos, Michael, and Vasileiou 17)

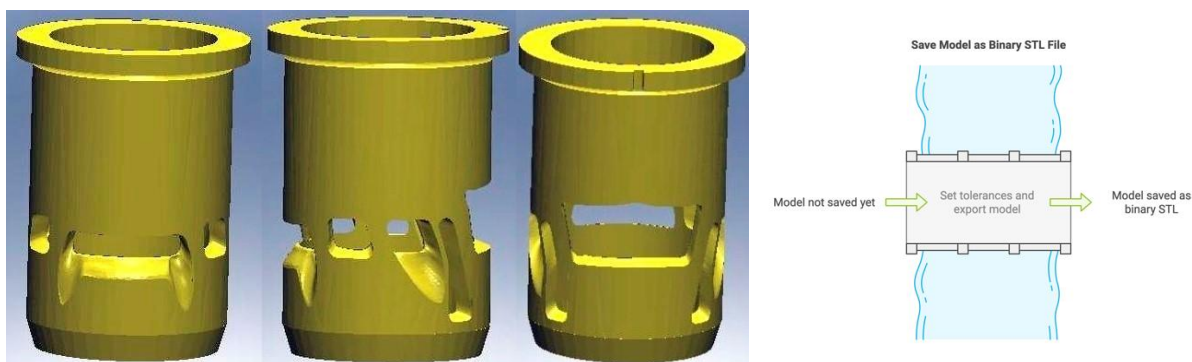


Figure 9. Part model (Vosniakos, Michael, and Vasileiou 17)

Material Investigation

To obtain the necessary specifications for casting, the material composition of the sample part was analyzed. The investigation was conducted using a Scanning Electron Microscope (JEOL 6390, JEOL Ltd, Tokyo, Japan) equipped with Energy Dispersive X-ray Analysis (EDX). Measurements were taken at multiple locations, including the bulk material and the thin coating layer on the inner cylindrical surface, to ensure the reliability and representativeness of the results, as illustrated in Figure 10a and Figure 10b, respectively.

The data obtained provided a detailed composition analysis of the part's material, which is critical for determining the appropriate casting process and ensuring that the replicated part

meets the original's performance standards. The results of the material analysis are summarized in **Table 1**.

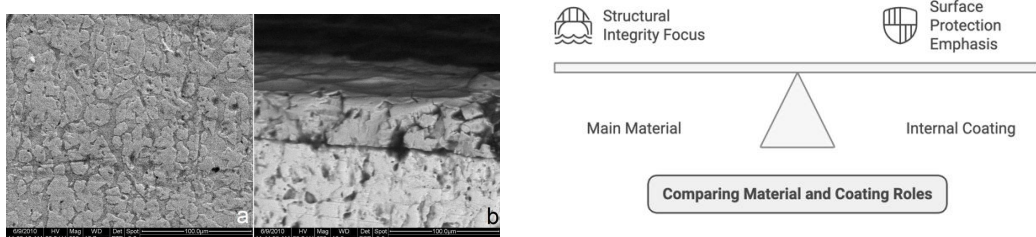


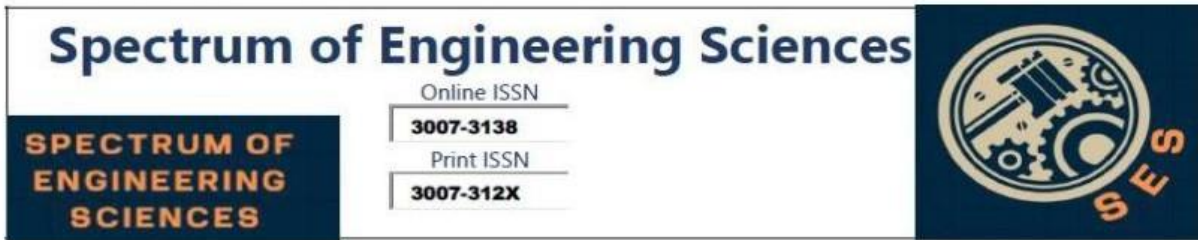
Figure 10. SEM micrographs (a) main material; (b) internal coating (upper layer) (Vosniakos, Michael, and Vasileiou 17)

Table 1. Scanning Electron Microscopy Results (Vosniakos, Michael, and Vasileiou 17)

Element	C	Cu	Zn	C	O	Si	Cr
Region	Mai n Bod y	Mai n Bod y	Mai n Bod y	Coat in g	Coat in g	Coat in g	Coat in g
Weight %	4.49	61.40	34.11	13.82	16.59	0.86	68.73
Atomic %	20.06	51.91	28.03	32.50	29.29	0.86	37.34

It was established that the liner consists mainly of copper and zinc, i.e., a brass alloy. A low percentage of carbon found is considered to be due to combustion residuals.

The coating consists of chromium and is usually applied for reasons of resistance primarily to wear and secondarily to corrosion. According to the scale depicted in Figure 10 b coating thickness is 44 μm.



Casting Simulation

Casting simulation was conducted using Procast™ (ESI Group, Paris, France), a robust software platform capable of simultaneously addressing thermal, fluid flow (mold cavity filling), and mechanical stress problems. The primary objective of the simulation was to test various vacuum casting parameters and feeding alternatives before implementing the process physically.

Simulation Setup

The digital model was scaled by 1.5% for brass shrinkage [31]. A finite element tetrahedral mesh was generated for the casting and mold, with mesh quality regulated by the delta value. Values between 0.8–0.9 ensured accurate geometry, while values over 1.0 caused loss of critical details.

Mold design was done either automatically (Virtual Mold) or manually, where the user defined the mold, element sizes, and mesh density. Mesh density was adjusted based on temperature variation in different regions to optimize simulation time.

The mesh size directly influenced file size and simulation time. For instance, 1.5 million elements resulted in a 700 MB file size and 11 hours of simulation time, while 0.5 million elements reduced the file size to 250 MB and simulation time to 2 hours.

Mesh quality was verified and corrected manually for problematic triangles (Figure 11a), with the final mesh shown in Figure 11b.

Mesh Sensitivity Analysis

A traditional mesh sensitivity analysis to find the coarsest mesh with consistent results was not feasible. Coarse meshes failed to converge, while very dense meshes exceeded system memory limits. Thus, a relatively dense mesh was chosen to balance functionality and reasonable simulation times.

The final mesh had high density in the casting region and coarser density towards the mold's external surfaces. Mesh sensitivity was evaluated using three criteria:

- 1. Solidification Time**
- 2. Cooling Rate**
- 3. Porosity**

These parameters were measured at two critical nodes: one near the port and another on the cylinder surface. The mesh was considered acceptable if these parameters remained consistent across multiple iterations, ensuring reliable results without overburdening computational resources.

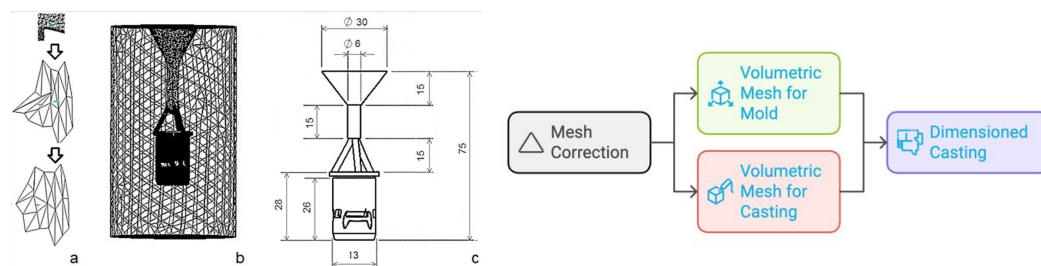


Figure 11. (a) Mesh correction: unacceptable triangles clipping to desired nodes and smoothing; (b) the two volumetric meshes for mold and casting, respectively; (c) Dimensioned casting with feeding system (units in mm) (Vosniakos, Michael, and Vasileiou 17)

After meshing is completed materials need to be assigned, in this case plaster for the mold and brass CuZn33 for the casting. Their properties are retrieved from the database available in Procast™. As described in Section 4, two different alloys are present: a copper alloy for the main material, and a chromium alloy

for the coating. To model the casting of the copper alloy, temperature dependent material properties are required. This information is not available in the literature. ProCAST features a database of certain materials, including pure copper (Cu), pure zinc (Zn) etc. Based on the chemical composition of Table 1, rule of mixtures is applied to result in the “calculated material properties” of this particular copper alloy. The calculated material properties presented in Figure 12 include temperature-dependent density, thermal conductivity, specific heat, viscosity, as well as the characteristic temperatures (Liquidus–Solidus). The Liquidus temperature used was 931 °C and Solidus was 886 °C (see Figure 12, solid fraction curve), and the latent heat was 205 KJ/kg. In brief, the SEM/EDX information is fed into the model.

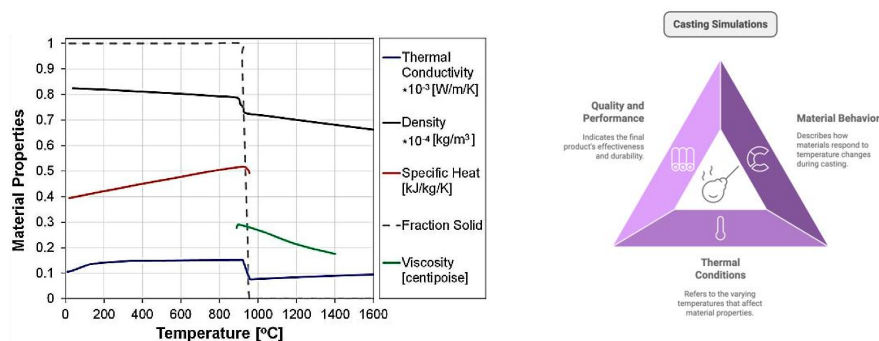


Figure 12. Temperature-dependent material properties used for the casting simulation (Vosniakos, Michael, and Vasileiou 17)

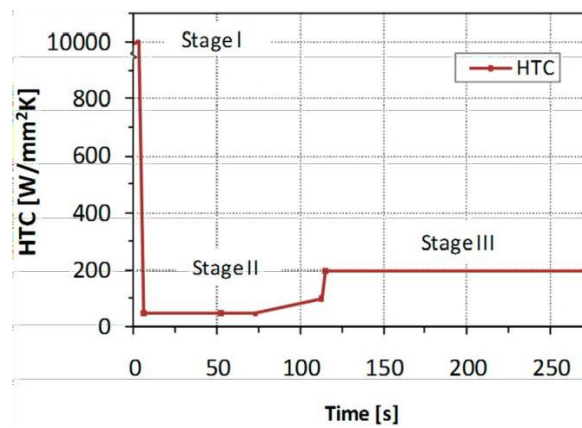
The interface characteristics, specifically the heat transfer coefficient (HTC) between plaster and brass, were assigned based on experimental data (Figure 13). The HTC follows a three-stage pattern:

Stage I: High HTC (initial 2.5 s), representing intense heat flow as molten metal contacts the mold.

Stage II: HTC drops to around 45 W/mm²K due to air gap formation during solidification.

Stage III: HTC slightly increases as solid-to-solid contact occurs under vacuum conditions.

This time-dependent behavior is typical in the literature [31] and depends on materials, casting conditions, and geometry. The HTC used here was calculated using the methodology from [23].



Plaster-Brass
Heat Transfer
Coefficient



heat transfer



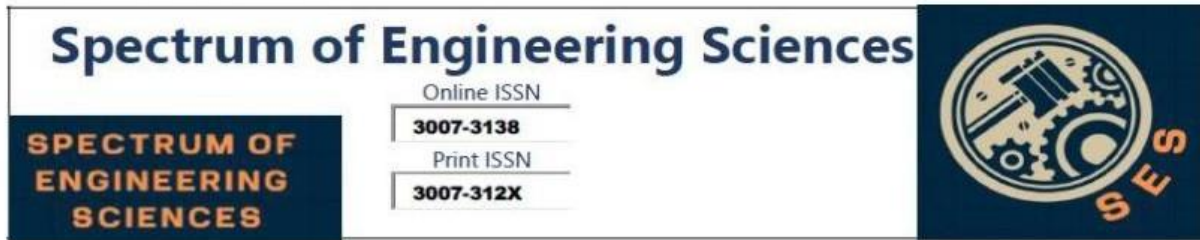
time



coefficient

Figure 13. Plaster-Brass Heat Transfer Coefficient as a function of time, according to [20,23].

Boundary conditions include setting temperature at specific nodes or node groups, i.e., on the mold external surface, as well as melt pouring velocity or mass flow rate (approximated using Bernoulli equation at 1.10672 Kg/s) and pressure at the mold-casting interface (0.03 bar for vacuum casting) and on the outer

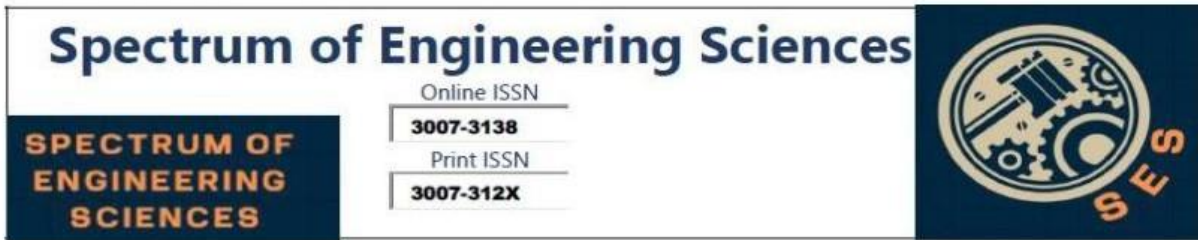


surface of the mold (1 bar). Initial conditions concern mainly initial temperature of the mold and the melt.

Furthermore, computational process parameters referring to numerical solution procedure were set according to the software guide rules [30].

Methodology

This study explores the relationship between transportation infrastructure, supply chain strategies, and operational efficiency in



the mining industry. It aims to identify key factors that enhance mining supply chain management, with broader applications for industries like energy, manufacturing, and construction. The outcomes will provide actionable strategies for improving cost-effectiveness and operational efficiency.

A mixed-methods approach will be used, consisting of:

Systematic Literature Review: Reviewing academic and industry reports to establish current knowledge and best practices.

Quantitative Data Analysis: Analyzing operational metrics, cost data, and performance indicators to evaluate supply chain efficiency.

Qualitative Research: Conducting interviews and focus groups with key stakeholders to identify challenges and opportunities.

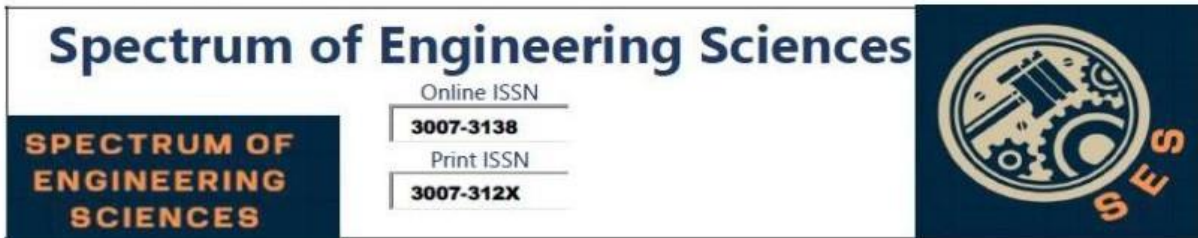
Case Studies: Examining successful mining supply chain initiatives to highlight critical success factors.

Simulation Modeling and Scenario Analysis: Using models to evaluate the impact of transportation investments and supply chain strategies on efficiency and cost.

This research aims to offer a comprehensive understanding of how transportation infrastructure impacts mining supply chain optimization, with insights for industry stakeholders and policymakers.

Results

Three sets of digital experiments were performed, namely (i) a set with fixed mold temperature in which three different feeding system designs and two different mold temperatures were tried (ii) a set with a fixed feeding system and a melt temperature selected from the previous set, in which three mold temperatures were tried (iii) a fixed case selected from the second set of experiments in



order to simulate in detail shrinkage and dimensional accuracy of the casting. The full set of conditions examined is presented in Table 2.

Digital Experiment Set	1	2	3	4	5	6	7	8	9	10
Number of Runners	3	3	4	4	5	5	5	5	5	5
Melt Temperature (°C)	970	1000	970	1000	970	1000	1000	1000	1000	970
Mold Temperature (°C)	730	730	730	730	730	730	660	730	800	730

Table 2. Full Set of Digital Experiments Performed Different Feeding System and Melt Temperatures (Vosniakos, Michael, and Vasileiou 17)

For a fixed mold temperature at 730 °C two melt temperatures, i.e., 970 °C and 1000 °C, were tried each on a different feeding system consisting of 3, 4 and 5 runners. The results concerning porosity are shown in Figure 14. Porosity is reduced as the number of runners increases. At the melt temperature of 1000 °C porosity is generally lower but the number of local defects (voids and porosity) near ports increases. The five-runner case is obviously better than the other two.

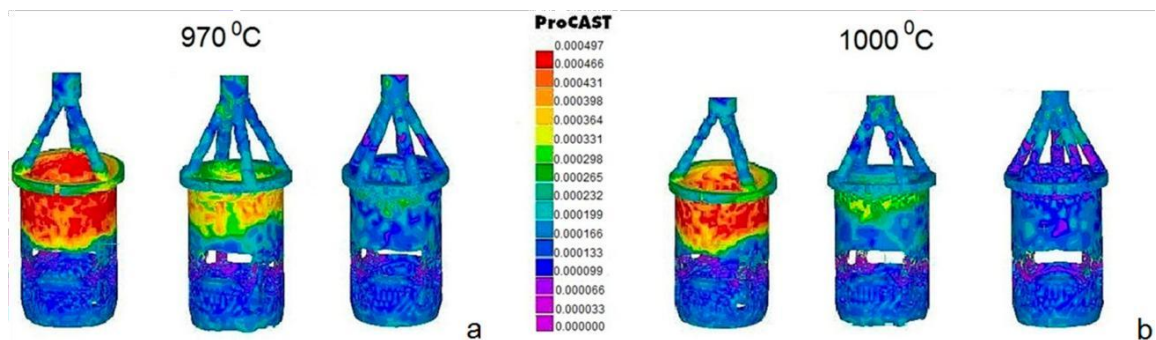
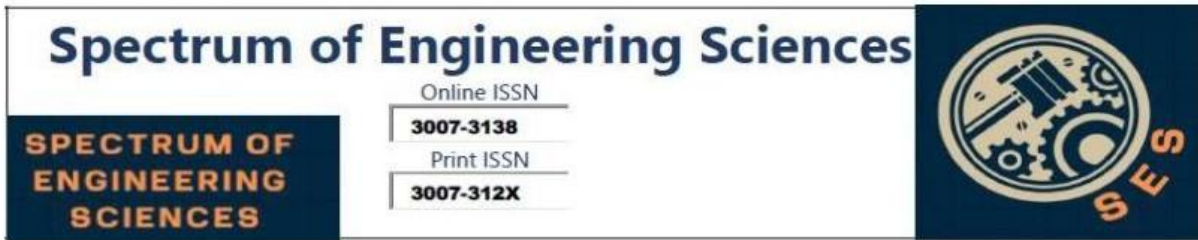


Figure 14. Porosity for melt temperatures (a) 970 °C and (b) 1000 °C and three feeding alternatives (Vosniakos, Michael, and Vasileiou 17)

Ased on previous experience, casting conditions outside the temperature range presented in this study often resulted in incomplete filling (e.g., melt temperature ~950 °C) or significant surface oxidation (e.g., melt temperature >1000 °C). Therefore, temperatures of 970 °C and 1000 °C were chosen as potentially viable conditions. It is important to note that the temperature difference between the melt and the mold is the critical factor. The objectives for the trials were to determine casting parameters that would produce a faithful reproduction of the casting shape, minimize oxidation or burn-outs, achieve acceptable levels of porosity, and ensure reasonably low solidification time.

Taking the five-runner case at a melt temperature of 1000 °C, three mold temperatures were tested: 660 °C, 730 °C, and 800 °C. Figure 15 presents the results in terms of solidification time and porosity. The selection criteria for the optimal mold temperature included:

- (1) Porosity levels within an acceptable limit, set at 0.01 to avoid macroporosity (as per the simulation software user guide [30]).
- (2) Uniform porosity distribution within the cast part, excluding the feeding system.
- (3) Consistent solidification time throughout the cast part volume.



(4) Avoidance of gaps or voids, particularly in critical regions such as the “ports.”

The results clearly show that a mold temperature of 730 °C achieved the best performance. At 800 °C, the melt cooled slowly, with solidification beginning at the runner outlet while the inner part of the casting remained in the liquid-solid phase for an extended period. This prolonged state led to significant macroporosity, particularly in the inner sections of the part. At 660 °C, while macroporosity was less severe, porosity remained concentrated at the top of the casting near the runner outlet, affecting uniformity.

Porosity levels across all conditions were generally low, with values below the macroporosity threshold of 0.01. However, the effect of casting parameters on porosity distribution was evident, with certain locations showing a tendency for porosity formation. Despite the low overall porosity, the uniformity of porosity and solidification time was critical in selecting the optimal scenario. Micro-porosity, observed in all cases, indicated acceptable casting quality.

In conclusion, the mold temperature of 730 °C offered the best balance between solidification uniformity, porosity control, and defect minimization, making it the most suitable choice for high-quality casting in this study.

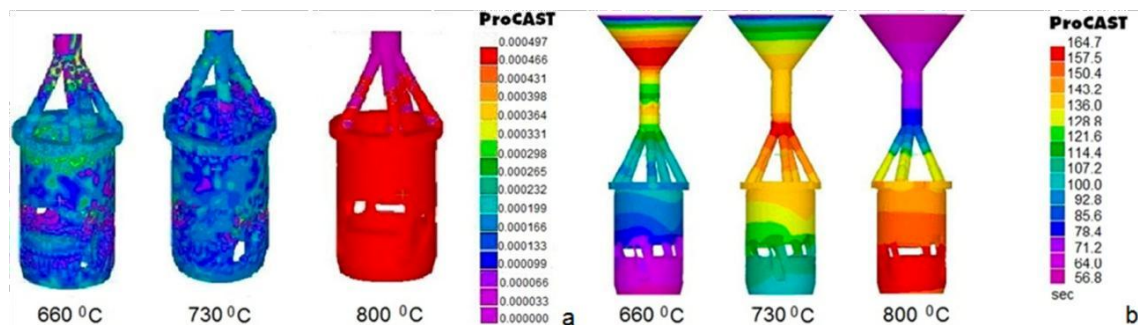
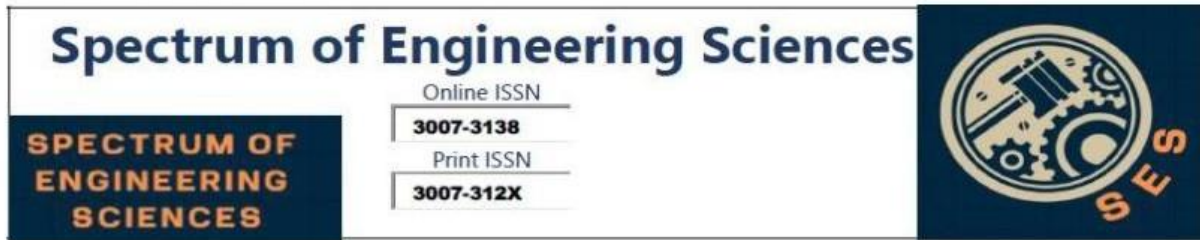


Figure 15. Best feeding alternative for three mold temperatures (a) Solidification time; (b) Porosity (Vosniakos, Michael, and Vasileiou 17)

Stress and Distortion for the Best Casting Case

For a five-runner system with a melt temperature of 970 °C and a mold temperature of 730 °C, identified as a favorable combination, shrinkage distortion of the casting was simulated from the beginning of the process down to room temperature. Two distinct boundary conditions were applied during the simulation: standard vacuum conditions for the initial 511 seconds, followed by full atmospheric conditions during cooling in water at 15 °C. This transition represents the standard practice in investment casting, where the flask is removed from the vacuum casting machine and immersed in water. The total displacement of the part is illustrated in Figure 16a, and the gap between the mold and casting caused by shrinkage is shown in Figure 16b.

The simulation results revealed a maximum displacement of 0.323 mm in the feeding system. Within the part itself, the maximum shrinkage displacement was significantly smaller, at 0.022 mm. However, displacement was not uniform across the part (Figure 16a). Areas with higher material concentration, such as regions with smaller ports, exhibited greater displacement, while areas underneath larger ports experienced reduced displacement.



The shrinkage-induced gap between the mold and casting was also examined (Figure 16b). The largest gap was observed at the conical end of the part, while minimal gaps were noted in the inner cylindrical section and beneath the ports. These observations highlight the non-uniform nature of shrinkage and its dependence on the geometry and material distribution of the casting. These findings are critical for understanding and mitigating potential defects in the final casting process.

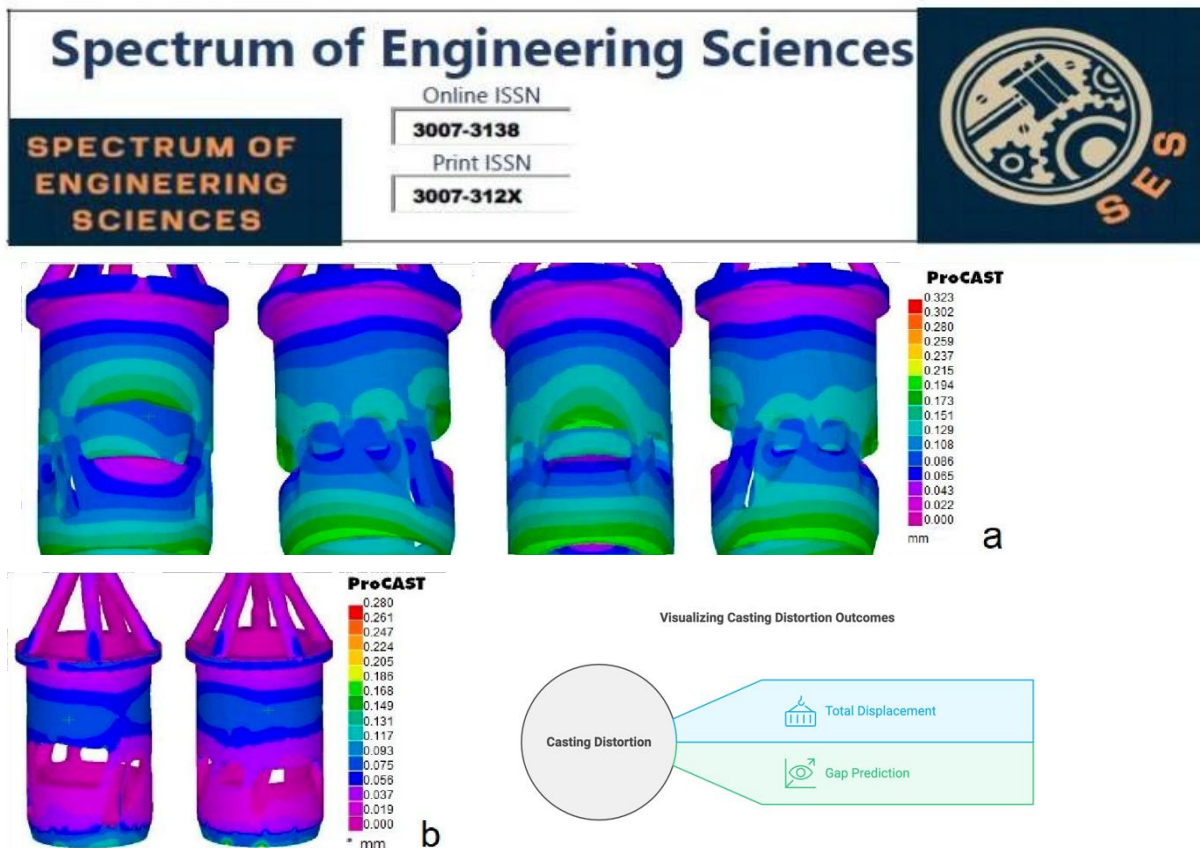


Figure 16. Casting distortion for the best casting case (a) Total displacement; (b) Gap prediction (Vosniakos, Michael, and Vasileiou 17)

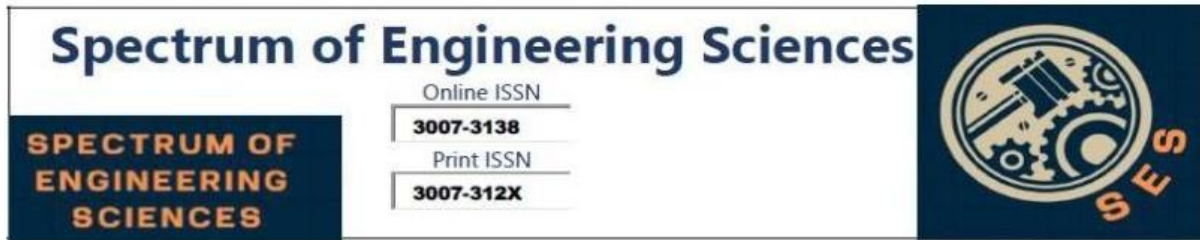
Casting Implementation

A standard lost-wax investment casting procedure was carried out [31], using the optimal parameters determined through casting simulation. The selected setup included a five-runner system, a melt temperature of 970 °C, and a mold temperature of 730 °C, as described in Section 5.

Procedure

For single casting production, a 3D printer can be used to create the casting model directly, eliminating the need for traditional dies. Due to the high resolution required, fabrication time is significant, necessitating the use of specialized 3D printers. In this study, a Solidscape R66™ (Solidscape, Inc., Merrimack, NH, USA), typically used for casting jewelry and dental restorations, was employed. The printer utilized wax-like resin materials designed for zero shrinkage and enhanced structural strength, making them ideal for precise casting patterns.

The produced wax model is displayed in Figure 17, where remnants



of the support structure are visible as darker areas. These supports were intentionally designed to stabilize the model during printing and were subsequently removed as part of the casting preparation process. This approach ensured the creation of a high-quality pattern suitable for investment casting.

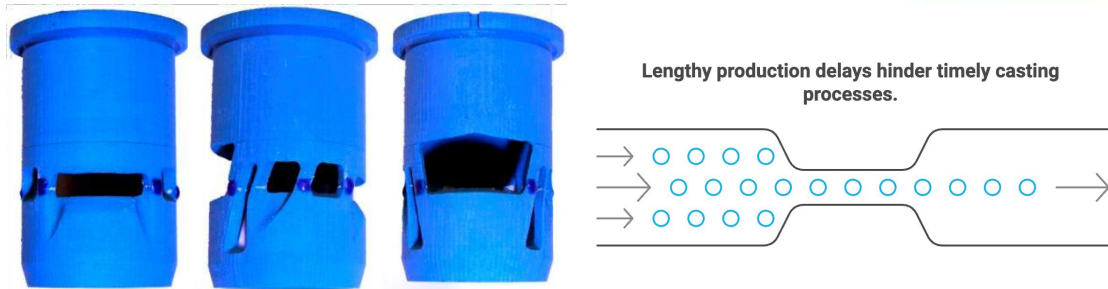
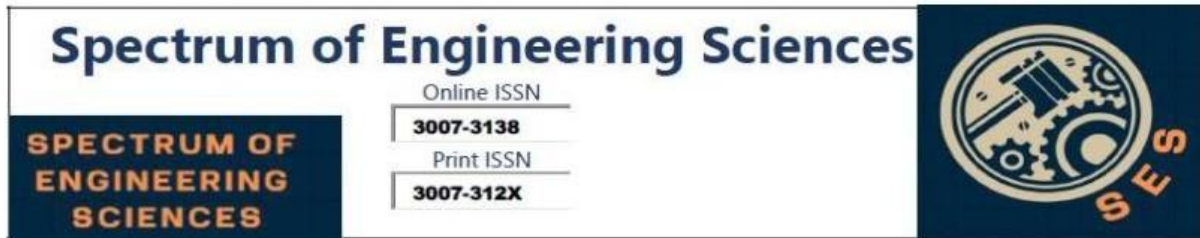


Figure 17. Wax model resulting from 3DP (Vosniakos, Michael, and Vasileiou 17)

The feeding system, comprising the sprue basin, sprue, and feeding runners, was constructed using standard wax components manually assembled with a soldering iron. This delicate process requires precision to ensure the stability of the assembly. The same method was employed to attach the feeding system to the wax model, forming the complete wax tree. In this case, the wax tree consisted of a single casting part.

Once the wax tree was prepared, it was mounted onto a rubber base (Figure 18a) and enclosed within a metal flask. Plaster (R&R Argentum Investment™, Ransom and Randolph, Maumee, OH, USA) was mixed with de-ionized water at a ratio of 100:39 by



weight, then de-aired for approximately 1.5 minutes (Figure 18b). The mixture was carefully poured into the flask to avoid direct contact with the wax tree and de-aired again for an additional 2 minutes (Figure 18c). De-airing was performed using a specialized machine equipped with a vibrating table to ensure bubble-free plaster (Figure 18d).

After approximately one hour, the plastered flask achieved sufficient hardness to be removed from the rubber base and placed in a dewaxing oven for 3.5 hours (Figure 18e). Subsequently, the plaster mold underwent additional heating in a separate oven (Figure 18f), first at 350 °C for 2 hours and then at 730 °C for 3.5 hours (as outlined in Section 5.2). The plaster material used has a shrinkage of less than 1.6% within the temperature range of 20–900 °C, with negligible shrinkage above 600 °C, ensuring the dimensional accuracy of the casting.

The casting process was carried out by placing the mold into a vacuum casting machine (Figure 18g). The appropriate amount of brass was melted in the machine's crucible and allowed to fill the mold cavity under vacuum assistance. After 8.5 minutes, the mold was removed from the machine and immersed in water, causing it to shatter and reveal the final casting (Figure 19a). This process ensured a high-quality reproduction of the part while maintaining dimensional accuracy and minimizing defects.

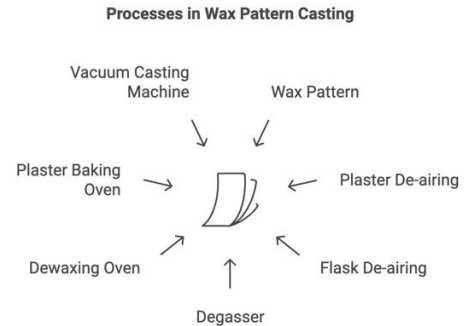


Figure 18. (a) Wax pattern with runners on rubber base before placement in the flask; (b) plaster de-airing; (c) flask de-airing; (d) degasser; (e) dewaxing oven; (f) plaster baking oven; (g) vacuum casting machine (Vosniakos, Michael, and Vasileiou 17)

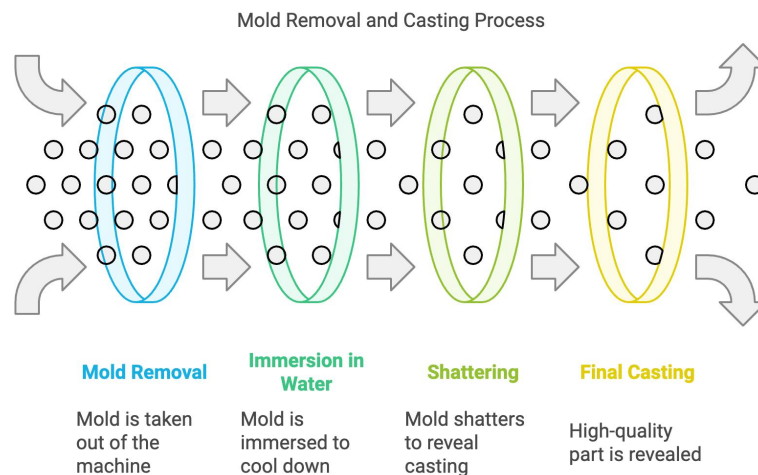
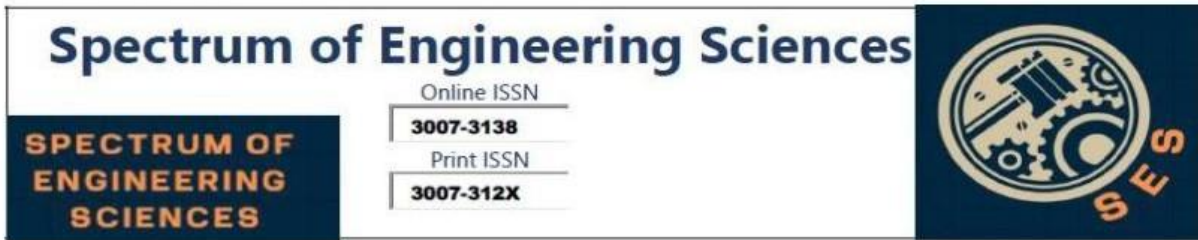


Figure 19. Casting (a) uncleaned tree (b) cleaned part (Vosniakos, Michael, and Vasileiou 17)

Casting Quality

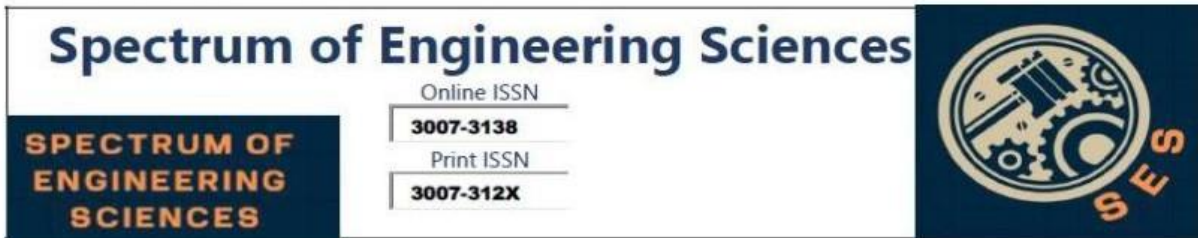
The final casting, after the removal of the feeding system and



thorough cleaning, is presented in Figure 18b. The accuracy of the casting was evaluated using the same Hawk™ laser scanner and procedures that were employed to scan the original part. Three specific measurement zones were analyzed:

- (1) A narrow stripe along the full height of the part.
- (2) Two areas on the external cylindrical surface.
- (3) A restricted area on the internal surface, as allowed by the opening.

These measurements were used to fit surfaces and determine the main dimensions of the casting. The comparison of the dimensions between the original part, the wax model, and the cast



copy is summarized in Table 3. The results show that the relative error of the cast copy compared to the original part is generally low, particularly for the height dimension, indicating a high level of dimensional accuracy.

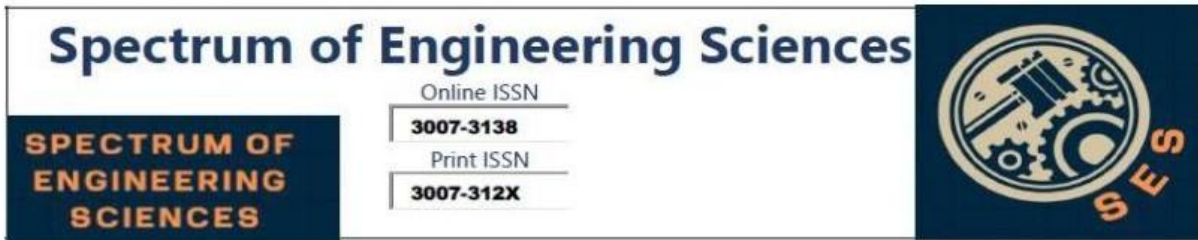
The surface finish of the cast part was measured using a Taylor Hobson Surtronic 3™ (AMETEK Inc., Berwyn, PA, USA). The average surface roughness was recorded as $R_a = 3.2 \mu\text{m}$, which is higher than the original part's $R_a = 1.2 \mu\text{m}$, highlighting the need for post-casting surface finishing to meet original standards.

Table 3. Main Dimensions of the Parts Constructed (Vosniakos, Michael, and Vasileiou 17)

Part	Height (mm)	External Diameter (mm)	Max Diameter (mm)	Internal Diameter (mm)
Original	30.400	9.750	8.204	
Wax	30.862	9.898	8.328	
Cast Copy	30.440	9.668	8.161	
Absolute Error (μm)	40	-82	-43	
Relative Error (%)	0.13	-0.84	-0.52	

Discussion

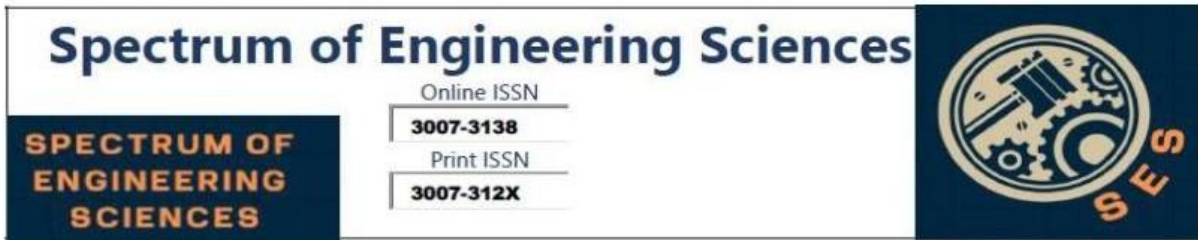
This study focused on examining the details and decisions involved in each stage of the process chain for producing one or very few castings based on a prototype to be replicated. The techniques used were assumed to be mature enough to deliver acceptable quality, as discussed in the "Introduction," provided they were applied correctly. The emphasis of this work was on ensuring proper application and decision-making to achieve desired outcomes.



A notable point regarding methodology is that, unlike many reverse engineering studies in the literature, this work did not scan a 3D-printed part and compare it with its digital model using color deviation plots. Similarly, the cast part was not scanned to compare deviations from the original prototype. Instead of focusing on validating the scanning, 3D printing, or casting techniques—each of which comes with manufacturer-guaranteed accuracy this study prioritized efficiency. In a production environment, repeating the scanning process twice (once for the printed part and once for the casting) is impractical and time-consuming. Instead, the approach focused on measuring main dimensions of the parts using conventional methods and scanning selected areas to provide a reliable indication of accuracy.

Part Digitizing

In addition to laser scanning, other technologies such as Coordinate Measuring Machines (CMM), optical scanning, and industrial computed tomography can be used to digitize parts. Laser scanning and CMM offer high accuracy, typically a few micrometers to 1 μm . However, while CMM provides structured point clouds, it is considerably slower than laser scanning. Optical scanning, using CCD cameras and structured light, captures thousands of points rapidly, making it much faster than laser scanning. However, optical scanning has reduced accuracy (typically 8–10 μm) and struggles with occlusion, making it less suitable for intricate parts with deep recesses. For small, complex parts like those in this study, laser scanning strikes the best balance between accuracy, time, and coverage. Scanning strategies, such as focusing only on the generatrix of a cylindrical part instead of the



entire surface, can further reduce scanning time without compromising accuracy.

Part Modeling

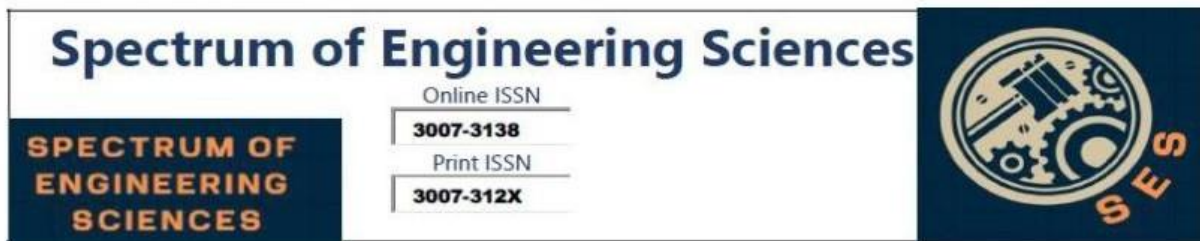
The process of fitting surfaces to point clouds can be time-intensive if an inappropriate strategy is adopted. Success depends heavily on experience, particularly regarding the point cloud's coverage and the geometry being reconstructed. When sufficient points are available, the primary concern is ensuring uniform digitization accuracy to avoid localized deformations. Conversely, if portions of the point cloud are missing, patching or repairing the model requires knowledge of the missing area's characteristics and continuity constraints. For surfaces with known geometries, the fitting process was straightforward, as expected.

Material Identification

Material identification remains a critical but often overlooked aspect of reverse engineering projects [18]. The process typically follows standard procedures, but additional challenges arise when multiple materials are combined, such as in coated parts. In such cases, sectional measurements must be taken, and techniques to measure layer thickness must be carefully chosen, often involving destructive methods. This makes material analysis particularly complex for coated components.

Virtual Casting

This study introduced casting simulation as a novel link in the digital manufacturing chain. Casting simulation proved invaluable in eliminating feeding system designs that were clearly unsuitable, allowing the focus to shift toward promising parameter combinations. While most literature on rapid casting emphasizes achieving a "right-first-time" outcome based on experience [1,2,5–



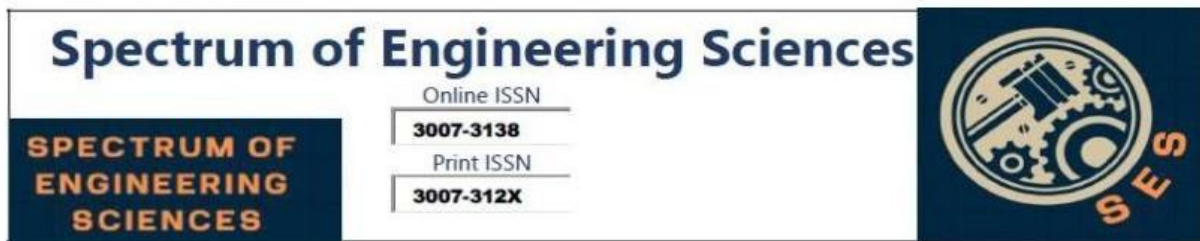
7,11,13,16,17,19,25,26,29], only a few studies [16,19,29] utilized simulation to validate a single proposed system. By contrast, this work advocates for using simulation to refine feeding system design and casting parameters iteratively.

It is important to note that this study did not aim to validate casting simulation itself. Instead, it relied on simulation models validated in other works, such as [20,23]. Simulation does not generate solutions autonomously but evaluates those proposed by the user. A potential pitfall in simulation is the heat transfer coefficient (HTC), which depends on the mold and casting materials and their shapes. HTC values must be adapted from similar cases in the literature or determined experimentally, a time-consuming process [23].

Casting Tool Construction

The casting procedure employed in this study is typical for jewelry casting, particularly for larger items with relatively few wax models on a single tree. For small batch production, the method of creating wax models via 3D printing followed by mold construction is effective, as the additional time required for mold preparation is minimal. This delay could be eliminated entirely by directly constructing the mold using additive manufacturing (AM) technologies. However, while advanced rapid casting systems often take this approach, the cost of creating ceramic molds with AM remains significantly higher than producing wax models [4].

The time required for wax tree construction via AM is comparable to the time needed to directly manufacture metal parts using Selective Laser Sintering/Melting. However, parts produced through precision casting generally exhibit superior surface quality compared to those manufactured via direct metal printing [1].



Variations in wax-based prototyping times are attributed to differences in the fundamental technologies employed by 3D printers, such as droplet size and spraying modes [4].

For larger production volumes, 3D printing may become cost-prohibitive. In such cases, metal patterns can be manufactured to create silicone rubber dies, which are then used to produce wax models. Alternatively, wax injection into dies may offer a more practical and economical solution for mass production [4].

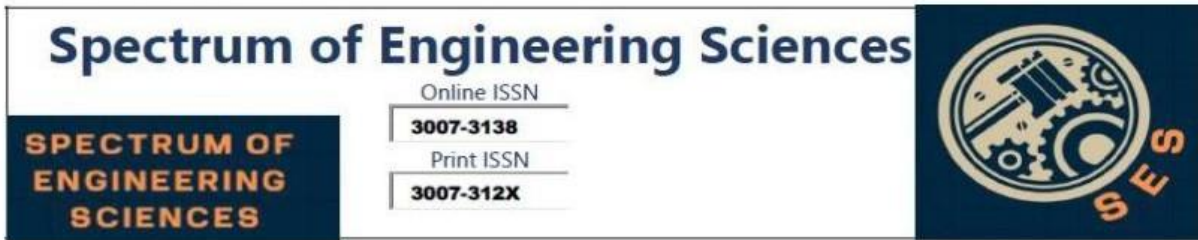
Conclusions

This study highlights the effectiveness of precision casting as a viable alternative to machining for producing small and intricate components, such as the cylinder liner investigated in this work. The digital manufacturing process chain developed and applied in this research incorporates critical steps, including accurate digitization of the original part, digital modeling using CAD software, material identification, casting simulation, wax model fabrication via additive manufacturing, manual mold construction, and precision casting. Each link in this chain requires careful execution to ensure successful replication of the original part.

The findings of this study suggest the following best practices for replicating single parts:

Accurate Digitization: Using a high-precision scanner, such as a laser scanner, is essential when sub-10 μm accuracy is required. Selective scanning of key areas instead of complete coverage significantly reduces scanning time.

Digital Model Reconstruction: Surface fitting and object reconstruction in CAD software must be optimized to ensure fidelity to the original geometry.



Material Analysis: Employing appropriate techniques, such as SEM, ensures accurate determination of material properties and specifications.

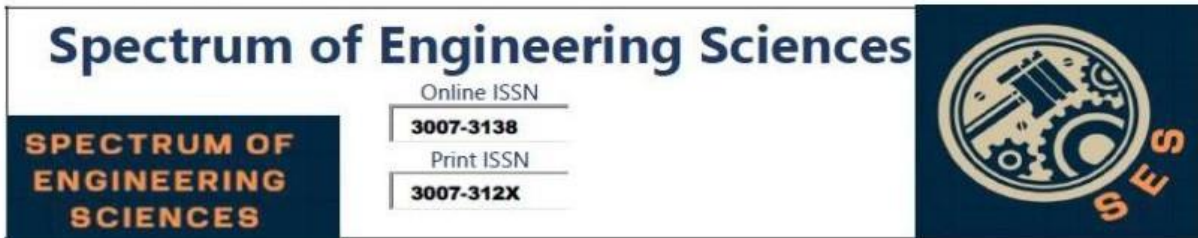
Casting Simulation: Validated simulation tools are indispensable for optimizing feeding system designs and casting parameters, reducing the need for extensive physical trials. Key criteria to evaluate casting quality include shape fidelity, porosity, solidification time, and shrinkage distribution.

Wax Model Fabrication: Wax or resin models created on 3D printers designed for casting provide the required precision and dimensional accuracy.

Casting Implementation: Automated vacuum casting machines minimize manual errors, although mold construction using plaster or similar materials remains a crucial manual task.

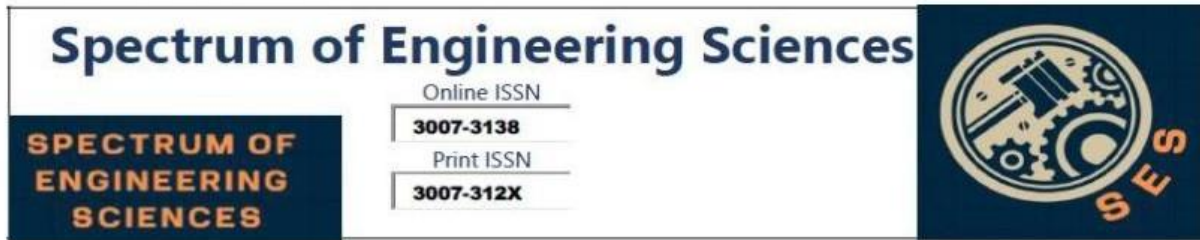
Among all stages, mold making is the most critical factor in achieving the desired part quality. However, the integration of digital tools at various stages significantly enhances the accuracy, efficiency, and reliability of the overall process chain.

In conclusion, the systematic application of digital manufacturing techniques combined with precision casting methodologies demonstrates the feasibility of producing high-quality one-off or limited-run components. This approach effectively leverages the capabilities of modern technology to meet the demands of complex part replication while minimizing time and resource consumption. These findings contribute to the broader adoption of precision casting as a reliable manufacturing technique for specialized applications.

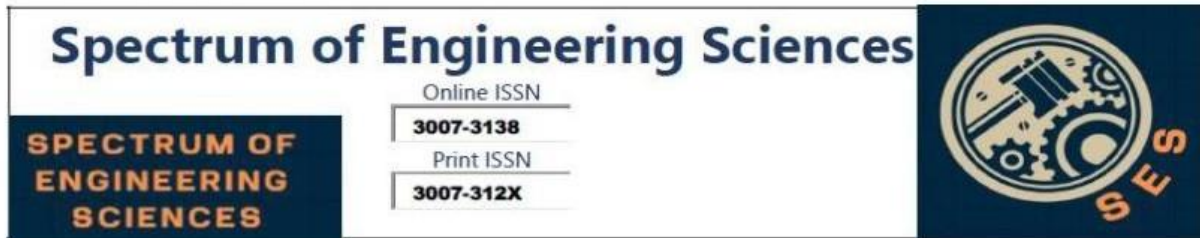


Reference

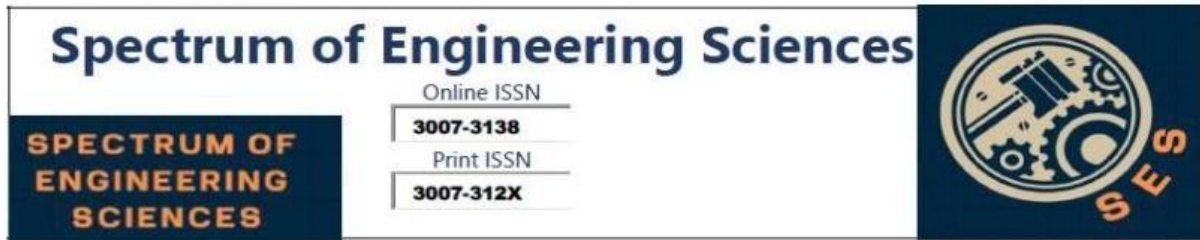
1. References: Karunakaran, K.P.; Bernard, A.; Suryakumar, S.; Dembinski, L.; Taillandier, G. Rapid manufacturing of metallic objects. *Rapid Prototyp. J.* **2012**, *18*, 264–280. [CrossRef]
2. Ramos, A.M.; Simões, J.A. CAD-CAM-RTV–lost-wax casting technology for medical implants. *Rapid Prototyp. J.* **2009**, *15*, 211–215. [CrossRef]
3. Cheah, C.M.; Chua, C.K.; Lee, C.W.; Feng, C.; Totong, K. Rapid prototyping and tooling techniques: A review of applications for rapid investment casting. *Int. J. Adv. Manuf. Technol.* **2004**, *25*, 308–320. [CrossRef]
4. Chhabra, M.; Singh, R. Rapid casting solutions: A review. *Rapid Prototyp. J.* **2011**, *17*, 328–350. [CrossRef]
5. Bassoli, E.; Gatto, A.; Iuliano, L.; Violante, M.G. 3D printing technique applied to rapid casting. *Rapid Prototyp. J.* **2007**, *13*, 148–155. [CrossRef]
6. Pal, D.; Ravi, B. Rapid tooling route selection and evaluation for sand and investment casting. *Virtual Phys. Prototyp.* **2007**, *2*, 197–207. [CrossRef]
7. Chua, C.K.; Feng, C.; Lee, C.W.; Ang, G.Q. Rapid investment casting: Direct and indirect approaches via model maker II. *Int. J. Adv. Manuf. Technol.* **2004**, *25*, 26–32. [CrossRef]
8. Pattnaik, S.; Karunakar, D.B.; Jha, P.K. Developments in investment casting process—A review. *J. Mater. Process. Technol.* **2012**, *212*, 2332–2348. [CrossRef]
9. Yarlagadda, P.K.D.V.; Hock, T.S. Statistical analysis on accuracy of wax patterns used in investment casting process. *J. Mater. Process. Technol.* **2003**, *138*, 75–81. [CrossRef]



10. Sabau, A.S.; Viswanathan, S. Material properties for predicting wax pattern dimensions in investment casting. *Mater. Sci. Eng. A* **2003**, *362*, 125–134. [CrossRef]
11. Ferreira, J.C.; Alves, N.F. Integration of reverse engineering and rapid tooling in foundry technology. *J. Mater. Process. Technol.* **2003**, *142*, 374–382. [CrossRef]
12. Liu, G.H.; Wong, Y.S.; Zhang, Y.F.; Loh, H.T. Modelling cloud data for prototype manufacturing. *J. Mater. Process. Technol.* **2003**, *138*, 53–57. [CrossRef]
13. Cheng, Y.; Wang, L.; Zhu, Z.; Zhang, D. Geometric analysis of investment casting turbine blades based on digital measurement data. *China Foundry* **2014**, *11*, 20–27.
14. Li, L.; Schemenauer, N.; Peng, X.; Zeng, Y.; Gu, P. A reverse engineering system for rapid manufacturing of complex objects. *Robot. Comput. Integr. Manuf.* **2002**, *18*, 53–67. [CrossRef]
15. Salvi, J.; Matabosch, C.; Fofi, D.; Forest, J. A review of recent range image registration methods with accuracy evaluation. *Image Vis. Comput.* **2007**, *25*, 578–596. [CrossRef]
16. Ferreira, J.C.; Mateus, A.S.; Alves, N.F. Rapid tooling aided by reverse engineering to manufacture EDM electrodes. *Int. J. Adv. Manuf. Technol.* **2006**, *34*, 1133–1143. [CrossRef]
17. Zhang, D.H.; Jiang, R.S.; Li, J.L.; Wang, W.H.; Bu, K. Cavity optimization for investment casting die of turbine blade based on reverse engineering. *Int. J. Adv. Manuf. Technol.* **2009**, *48*, 839–846. [CrossRef]
18. McEvily, A.J. Reverse engineering gone wrong: A case study. *Eng. Fail. Anal.* **2005**, *12*, 834–838. [CrossRef]



19. Bernard, A.; Delplace, J.; Perry, N.; Gabriel, S. Integration of CAD and rapid manufacturing for sand casting optimisation. *Rapid Prototyp. J.* **2003**, *9*, 327–333. [CrossRef]
20. Vassiliou, A.N.; Pantelis, D.I.; Vosniakos, G. Investigation of centrifugal casting conditions influence on part quality. *In Proceedings of the International Conference on Manufacturing Engineering*, Halkidiki, Greece, 1–3 October 2008; pp. 347–356.
21. Gramegna, N.; della Corte, E.; Poles, S. Manufacturing process simulation for product design chain optimization. *Mater. Manuf. Process.* **2011**, *26*, 527–533. [CrossRef]
22. Iqbal, H.; Sheikh, A.K.; Al-Yousef, A.; Younas, M. Mold design optimization for sand casting of complex geometries using advanced simulation tools. *Mater. Manuf. Process.* **2012**, *27*, 775–785. [CrossRef]
23. Vasileiou, A.; Vosniakos, G.; Pantelis, D. Determination of local heat transfer coefficients in precision castings by genetic optimization aided by numerical simulation. *Proc. Inst. Mech. Eng. Part C J. Mech. Eng. Sci.* **2014**, *16*. [CrossRef]
24. Singh, J.P.; Singh, R. Investigations for a statistically controlled rapid casting solution of lead alloys using three-dimensional printing. *Proc. Inst. Mech. Eng. Part C J. Mech. Eng. Sci.* **2009**, *223*, 2125–2134. [CrossRef]
25. He, J.; Li, D.; Lu, B.; Wang, Z.; Zhang, T. Custom fabrication of a composite hemi-knee joint based on rapid prototyping. *Rapid Prototyp. J.* **2006**, *12*, 198–205. [CrossRef]
26. Zhang, Y.; Liu, H. Application of rapid prototyping technology in die making of diesel engine. *Tsinghua Sci. Technol.* **2009**, *14*, 127–131. [CrossRef]



27. Wang, L.; Li, H.; Gui, Y.; Zhao, G. A rapid design and manufacturing system for product development applications. *Rapid Prototyp. J.* **2004**, *10*, 200–206.
28. Sokovic, M.; Kopac, J. RE (reverse engineering) as necessary phase by rapid product development. *J. Mater. Process. Technol.* **2006**, *175*, 398–403. [CrossRef]
29. Pal, D.; Ravi, B.; Bhargava, L.; Chandrasekhar, U. Rapid casting development using reverse engineering, rapid prototyping and process simulation. *Indian Foundry J.* **2005**, *51*, 23–34.
30. ESI Group. PROCAST v2004.1; ESI Group: Paris, France, 2004.
31. Campbell, J. *Castings-The New Metallurgy of Cast Metals*; Butterworth Heinemann: Oxford, UK, 2003.